Photothermal Single-Particle Microscopy: Detection of a Nanolens

Markus Selmke, Marco Braun, and Frank Cichos*

Molecular Nanophotonics Group, Institute of Experimental Physics I, Leipzig University, 04103 Leipzig, Germany

ABSTRACT

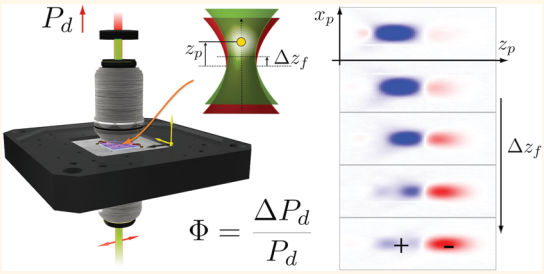

Combining quantitative photothermal microscopy and light scattering microscopy as well as accurate MIE scattering calculations on single gold nanoparticles, we reveal that the mechanism of photothermal single-molecule/particle detection is quantitatively explained by a nanolensing effect. The lensing action is the result of the long-range character of the refractive index profile. It splits the focal detection volume into two regions. Our results lay the foundation for future developments and quantitative applications of single-molecule absorption microscopy.

KEYWORDS: nanolens · photothermal microscopy · single-molecule detection · gold nanoparticle · optical microscopy · absorption · extinction · light scattering

The detection of single nano-objects by their luminescence has experienced an immense development during the last two decades.[1,2] Fluorescence-based microscopy of single molecules and nanoparticles has almost become a standard technique in physics, chemistry, and biology as it opens a window to the study of static or dynamic heterogeneity in the nanoworld. The rediscovery of photothermal contrast[3,4] has recently complemented these methods by the detection of nano-objects in absorption with a technique pioneered more than 30 years ago.[5,6] In contrast to fluorescence-based methods, the photothermal (PT) contrast arises from the release of heat by an absorber to its local environment. This increases the local temperature and modifies the refractive index in the direct vicinity of the absorber. The change of the refractive index can be well detected by optical means such as differential interference contrast[7] or the so-called photothermal heterodyne detection,[8,9] which has pushed sensitivity up to the level of single molecules.[10,11] The latter technique has been successfully applied to study the absorption spectra of single gold-nanoparticles, semiconductor nanoparticles, or carbon nanotubes. New techniques such as photothermal correlation spectroscopy complementing fluorescence correlation techniques or distance measurements by coupling two metal particles have been realized or put forward.[12−16] These recent developments highlight the perspective of photothermal microscopy to experience a similar success as single molecule fluorescence detection. However, most of the applications and their further development are considerably limited by the fact that neither a sound understanding of the photothermal signal generation process for single nanoscale absorbers nor a true description of the photothermal detection volume exists. Despite extensive literature describing the photothermal signal of ensembles of absorbers,[6,17] there is currently only one theoretical approach to photothermal signal generation for a point-like absorber[8] with a very limited predictive power.

Here we combine extensive single nanoparticle light scattering experiments and a complex theoretical scattering description to uncover the foundations of photothermal single molecule/particle detection. Our results highlight directly a number of new applications stemming from the unveiled unique shape of the signal.

A typical situation of photothermal single-particle detection is provided by a gold nanoparticle in the focus of a laser beam. Most of the absorbed electromagnetic energy by the particle is released as heat to the host material. This creates a temperature field which decays with the inverse distance r from the absorber[18]

$$\Delta T(r) = \Delta T \frac{R}{r} \qquad (1)$$

* Address correspondence to cichos@physik.uni-leipzig.de.

Received for review January 13, 2012 and accepted February 21, 2012.

Published online February 21, 2012
10.1021/nn300181h

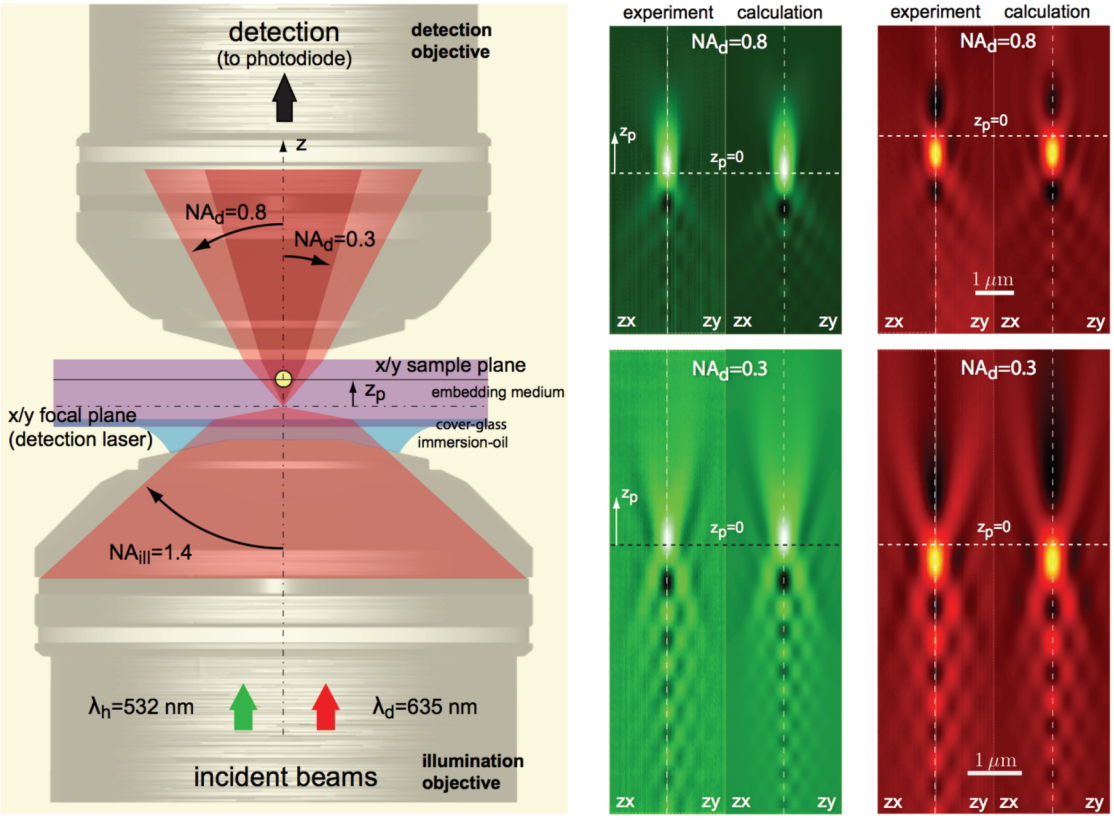

Figure 1. (Left) Schematic representation of the experimental setup used for the images (sample scanning). Shown is the particle position z_p, whereas x_p and y_p are the lateral directions (not depicted). (Center) Transmitted detected power P_d: Scattering of the heating laser on the gold-nanoparticle (AuNP, R = 30 nm). (Right) Scattering of the probe laser on the AuNP. The top row images represent the scans for a detection aperture NA_d = 0.8, the bottom row images NA_d = 0.3. The images are grouped experimental/theoretical scans.

where the temperature rise of the material directly adjacent to the particle surface $\Delta T = P_{abs}/(4\pi\kappa R)$ is resulting from the absorbed power P_{abs} and depends on the heat conductivity κ of the surrounding material and the particle radius R. An interfacial resistivity between the solvent and the particle has the effect of an increased particle temperature relative to this value but leaves the solvent temperature profile unchanged.[18] A corresponding refractive-index profile is thereby established, modifying the unperturbed refractive index n_m of the solvent to

$$n(r) = n_m + \frac{dn}{dT}\Delta T(r) = n_m + \Delta n \frac{R}{r} \qquad (2)$$

This infinite refractive index profile can be exploited to detect even a minute absorber with a probe laser in an optical microscopy setup with extremely high sensitivity.[3,11] However, the infinite size of the refractive index profile and the complex spatial structure of the tightly focused, aberrated laser beams cause some conceptual and computational challenges for a quantitative understanding of the signal generation,[8] which hampers further developments in this field. These are addressed below, where we develop a consistent formalism to quantitatively explain and analyze such "absorption microscopy" experiments in great detail. Our study allows the extraction of induced temperatures and thereby of absorption cross sections of single quantum systems from their photothermal signal. Moreover, understanding the details of the signal generation mechanism behind single-molecule photothermal microscopy will pave the way for further experimental developments for efficient room temperature single-molecule absorption spectroscopy.

RESULTS AND DISCUSSION

The complexity of the signal generation and local electromagnetic field distributions can be recognized when both involved lasers (heating and probe) scatter from a single gold nanoparticle at low incident power, where the heating is still negligibly small. The transmitted intensity collected by an objective lens reveals strong interference patterns as the particle senses the field structure of the aberrated incident laser beams (Figure 1, right). Recording these scattering intensities at different detection numerical apertures NA_d emphasizes the importance of the phase relation of scattered and transmitted electric fields. A larger numerical detection aperture decreases the amplitude of the detected interference structure around the main intensity peak. The interference patterns become less pronounced when the photothermal signal is considered. This is

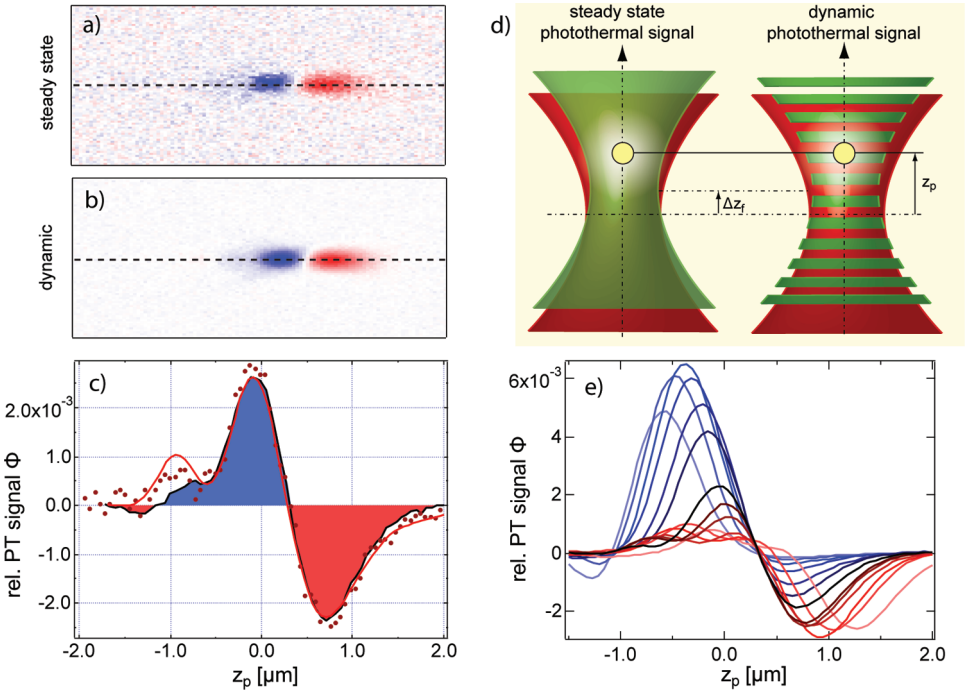

Figure 2. Difference of hot/cold NP scattering images: (a) Static difference image. (b) Dynamic PT signal recorded with a lock-in amplifier. (c) Comparison of axial PT dynamic (solid black)/static (red dots)/theoretical (solid red) scans. (d) Schematic of the displacement parameter Δz_f and the axial particle position z_p. (e) Experimental PT signal scans for different displacement parameters Δz_f.

because at low modulation frequencies ($\lesssim$1 MHz, depending on the thermal diffusivity of the medium[8]) the photothermal signal should directly correspond to the difference of the steady state probe laser scattering signal on a heated nanoparticle including the long-range refractive index profile and a nonheated particle without the refractive index change. Only at high heating laser modulation frequencies ($\gtrsim$1 MHz), does the finite heat conductivity κ of the surrounding medium prevent the temperature profile from establishing its steady state inverse distance dependence and the photothermal signal starts to deviate from the steady state difference.[8,18] In this case the photothermal signal is observed to strongly decrease with further increasing modulation frequency. Even with the consideration of a finite interfacial resistivity[19] the surrounding thermal conductivity is the limiting parameter for the build-up of the solvent temperature profile. To validate the steady state assumption for our experiments the scattering difference has been evaluated under steady state conditions, recording two scattering images as well as dynamically using the photothermal heterodyne technique (300 kHz modulation frequency)[8] for an axial focus displacement of both lasers of 350 nm (see Figure 2a,b). Despite the much lower signal-to-noise ratio of the steady state difference, both signals agree perfectly (Figure 2c). Consequently, a steady state approach will be sufficient to model the photothermal signal in the second half of this paper. The experimental data displays a simple photothermal signal shape along the optical axis with a positive and negative signal lobe (Figure 2c). The two-lobe structure suggests a much simpler mechanism than the complex aberrated spatial heating and probe laser scattering intensity distributions put forward. It also demonstrates the fact that the assumption of a product point spread function of heating and detection laser is not appropriate to describe the photothermal focal volume. Instead, the two-lobe structure and the emphasis of the two lobes depend sensitively on the axial displacement Δz_f of the two laser foci (Figure 2d,e). However, independently of Δz_f, whenever the probe laser focus is in front of the refractive index profile, the detected intensity is decreased as compared to the undisturbed probe beam, while an increased signal is measured if the probe laser focus is behind the refractive index profile, as indicated in Figure 2c. This corresponds to the action of a diverging gradient index lens determining also the signal in the macroscopic counterparts of thermal lens spectroscopy.[6,17] The divergent lens is a result of the negative thermorefractive coefficient ($dn/dT < 0$), which lowers the local refractive index according to the local temperature rise $\Delta T(r)$.

A striking feature of the detected photothermal signal is that both lobes are disjunct and sharply separated. A particle either causes a positive or a negative photothermal signal, depending on its position relative to the focus of the probing beam. Further, the photothermal signal varies approximately linear

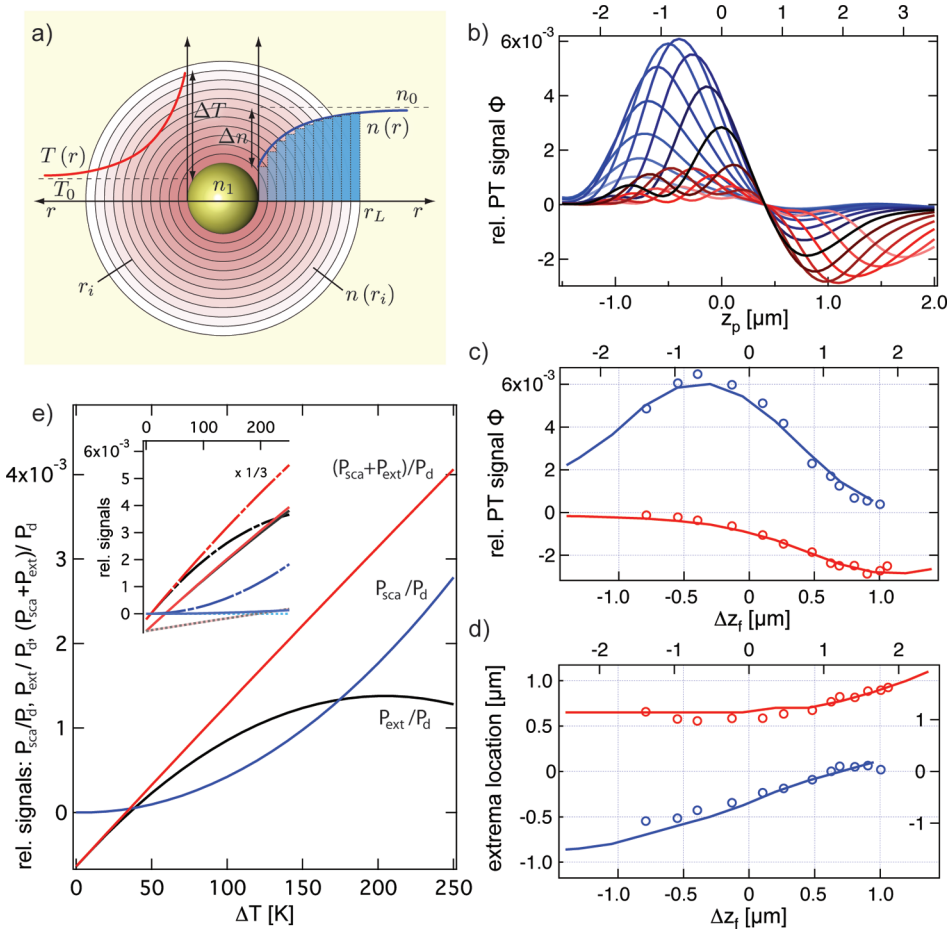

Figure 3. (a) Illustration of the temperature profile $T(r)$, the refractive index profile $n(r)$, and the discretization of the latter. (b) Theoretical photothermal z_p scans for varying foci displacements Δz_f for $R = 30$ nm AuNP. (c) Peak amplitudes *vs* Δz_f. Top axes are normalized coordinates, that is, $\Delta z_f/z_{R,d}$. (d) Peak positions *vs* Δz_f. Right axis is the position normalized to $z_{R,d}$. (e) Signal power-decomposition for a $R = 10$ nm AuNP and $\Delta z_f = 0$ at the maximum signal position ($z_p = -300$ nm): P_{ext}/P_d (black), P_{sca}/P_d (blue), $(P_{ext}+P_{sca})/P_d$ (red). The inset shows these for $n(r) = n_m + \Delta n \exp(-(r-R)/(2R))$ (dotted, bright red solid), $n(r) = n_m + \Delta n \exp(-(r-R)/(4.5R))$ (solid), $n(r) = n_m + \Delta n \exp(-(r-R)/(10R))$ (dashed-solid).

with the axial particle position z_p within a range of 200 nm around the inflection point. The slope of this linear part is within certain bounds ($-0.4\ \mu m < \Delta z_f < 0.1\ \mu m$) independent of the defocusing Δz_f. Thus, the particle position is directly proportional to the signal. This provides the advantage, that any photothermal signal fluctuation in this linear regime directly reveals the fluctuations in the axial position except for a constant factor. This yields remarkable perspectives for measuring small amplitude motions or even small particle displacements, such as in biological samples. The sharp separation of the two lobes also considerably extends recently developed photothermal correlation spectroscopy techniques.[12] Besides the commonly calculated autocorrelation of the signal magnitude, cross-correlations of positive and negative signals become accessible and allow for the detection of anisotropic and directed motion with unprecedented accuracy (to be published). Accordingly, it is apparent that the careful control and understanding of the photothermal signal generation mechanism would provide great value for these applications or even pave the way for new developments.

To gain a deeper insight into the photothermal signal generation we stress a rigorous scattering description to demonstrate that an exact electromagnetic treatment provides the above anticipated picture of nanolensing. This theoretical scattering description has to go beyond common MIE theory as photothermal microscopy employs highly focused laser beams instead of plane waves. We have therefore extended a rigorous MIE description (generalized Lorenz-MIE theory, GLMT[20]) to account for the axial structure of the signal and to accurately model aberration effects in the focused laser beams.[21,22] Our approach further includes the interaction of the aberrated laser fields with the metal particle and most importantly the refractive index profile, as point-scatterer descriptions[23] will not accurately model the situation at hand. The latter one is introduced in a multiple shell approach discretizing the refractive index profile as described by Peña et al.[24] (see Figure 3a). As a first check

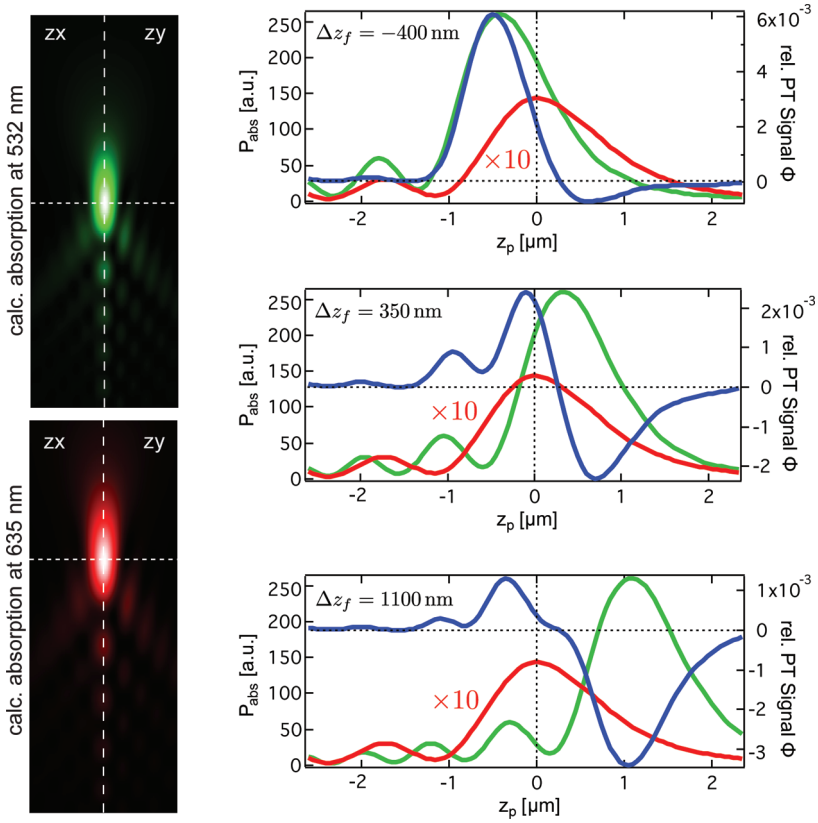

Figure 4. Left column: Calculated scans of the absorbed power P_{abs} (∝ point spread function, $|E|^2$) for the heating laser (top) and the detection laser (bottom). Right column: Representative scenarios for the relative alignments of the two lasers: (top) maximal positive photothermal signal, (center) symmetric signal, and (bottom) maximal negative signal. Plotted are the heating beam (green, fluorescence) and probe beam (red) intensities as well as the resulting photothermal signals (blue) *vs* the axial particle (R = 30 nm AuNP) coordinate z_p.

of the theoretical approach we model the scattering of the heating and probe laser on a single gold nanoparticle corresponding to the experimental data above. Incorporating the experimental and material parameters (see the Methods section and the Supporting Information) into the scattering calculations unveils a remarkable quantitative agreement with the experimental results (see Figure 1). The obtained axial scattering images (*xz*- and *yz*-plane) are largely determined by aberrations of the incident laser fields (see Figure 4) and additional interference structures. The found positions of maximum scattering intensity and incident laser focus do not coincide and strongly depend on wavelength. While both positions differ only slightly for the heating laser at $\lambda_h = 532$ nm they deviate notably at the detection wavelength of λ_d = 635 nm. This displacement of peak scattering signal and incident focus position is the result of the interference of scattered and incident laser fields and thus the result of a variable phase shift between both fields close to the resonance. While on resonance or at lower wavelengths the scatter-signal scans show a simple dip profile, a dispersion-like feature appears around the particle position for longer wavelengths. This feature is found to be more pronounced for lower numerical detection apertures, longer wavelengths, and stronger focusing. Further, the spatially extended incident intensity distribution causes the peak intensity in both laser foci to be much lower than for a Gaussian beam having a beam-waist of the corresponding diffraction limit (∼0.61 λ/NA_{ill}). As compared to such a Gaussian beam only one-third of the particle temperature is reached in the system studied here. Common temperature approximations therefore overestimate the actual particle temperature due to aberrations in the incident heating laser intensity distribution. Similar arguments apply to the detection laser intensity distribution. The amplitude of the interference pattern in the scattering images is further determined by the numerical aperture of the detection lens as found in the experiment. The larger this detection aperture is, the weaker the interference patterns get as the individual phase differences at different detection angles average out (Figure 1, right). This finding confirms that the plane wave optical theorem is not applicable when collecting signals at finite detection angle and focused illumination.[25] The only way to conclude on the intensity distribution details in the scattering experiment is to consider the finite detection angle and the higher order multipoles in the field expansions.

While the complex interference pattern determines the shape of the scattering intensity distribution, a

contribution to the photothermal signal is also expected[6,17] but less obvious. According to our experiments, the photothermal signal can be evaluated as the difference between the probe scattering intensity distribution of a particle with the refractive index profile and without the profile (low frequency limit). As a result of this difference, almost all of the interference structure of the above displayed scattering signals disappears. Only the phase advance in the probe field due to the generated refractive index profile leads to a change in the angular intensity distribution (to be published). This results in a simple two-lobe structure, which exactly corresponds to our experimental observations (Figure 2c) without any additional fitting parameter. Even the dependence of the total signal on the displacement of the two involved laser foci Δz_f is reproduced, which validates our GLMT approach (Figure 3b). This demonstrates that a quantitative analysis of photothermal microscopy data in terms of temperatures, absorption cross sections, and even in terms of the sign of the thermorefractive coefficient dn/dT is possible. A positive thermorefractive coefficient would invert the observed photothermal signal due to the convergent gradient index lens generated. Positive and negative thermorefractive coefficients occur for instance in liquid crystalline materials, characterizing the phase state of the liquid crystal at a well-defined temperature. An immediate consequence is that, for instance, local phase transitions, which occur on length scales of a few nanometers, become accessible as they typically involve strong refractive index changes. The experimental and theoretical treatments presented here thus open a field of new nanoscale material studies by photothermal microscopy.

Here, we further pursue an analysis of the signal generation process itself. The mechanism of photothermal detection is commonly explored by theoretically separating the total electric field $\mathbf{E}$ into contributions of an incident probing field $\mathbf{E}_{pr}$ and an outgoing scattered spherical wave $\mathbf{E}_{sca}$. Inserting $\mathbf{E} = \mathbf{E}_{pr} + \mathbf{E}_{sca}$ (and $\mathbf{H}$) into the expression for the forward-detected energy-flux,

$$P_d = \int_{\mathcal{A}_d} \langle \mathbf{S}(\mathbf{r}) \rangle_t \cdot d\mathbf{A} = \frac{1}{2} \int_{\mathcal{A}_d} \mathcal{R}(\mathbf{E}(\mathbf{r}) \times \mathbf{H}^*(\mathbf{r})) \cdot d\mathbf{A} \quad (3)$$

that is, the time-averaged Poynting vector $\langle \mathbf{S} \rangle_t$ integrated over an area $\mathcal{A}_d$ representing an angular detection domain, the detected power P_d mathematically decomposes into three separate integrals:[26] the probe laser background signal P_{pr}, the scattering signal P_{sca} and the extinction signal P_{ext} comprising an interference of probe $\mathbf{E}_{pr}$ and scattered field $\mathbf{E}_{sca}$. The photothermal signal is then calculated by taking the difference of single-particle scattering images in the presence and absence of the refractive index profile at the probe beam wavelength. This signal is then normalized to the scattering background in the images without the refractive index profile. Separating scattering and interference contributions to the relative photothermal signal $\Phi = \Delta P_d/P_d$ in our numerical results reveals that both parts change in a nonlinear way with increasing nanoparticle temperature independent of the nanoparticle size (Figure 3e shows a computation for a AuNP close to the Rayleigh size-regime). It is only their sum that grows linearly with the absorbed heating power (see Figure 3e). This nonlinear contribution of scattering and interference to the total signal varies with the numerical detection aperture. At low numerical detection aperture (*i.e.*, $NA_d \approx 0$) the photothermal signal is extinction-dominated. Thus the interference contribution rises linearly with the heating power absorbed by the particle. This situation, however, is experimentally unfavorable since the collected power at the photodiode decreases with decreasing numerical detection aperture as well as the signal-to-noise ratio. At higher numerical apertures (*i.e.*, $NA_d = 0.8$), the interference contribution determines the photothermal signal up to a temperature rise of about 50 K. Above this temperature scattering contributes more than 10% and increases strongly. Therefore, the scattering intensity from the refractive index profile is relevant to a number of experiments[12,13,27,28] and cannot be neglected for quantitative data analysis. The nonlinear dependence of scattering and interference contributions to the total signal at moderate temperature rises is directly related to the inverse distance dependence of the refractive index change which involves a diverging length scale. A leading contribution of the interference term is, however, found when considering a gold particle surrounded by an artificial refractive index profile decaying exponentially on a length scale of twice the particle radius $2R$. Increasing that length scale to $10R$ and thus beyond the focal beam waist reveals similar nonlinearities as observed for the inverse distance dependence of the refractive index, while a length scale of $4.5R$ yields the same magnitude, while showing already the onset of the nonlinearity. It is thus the divergent length scale of the refractive index profile around the point-like absorber, which makes the scattering contribution relevant even at moderate temperature rises and photothermal detection highly sensitive. It also follows from this consideration of different refractive index profiles, that a calibration of the photothermal signal for the measurement of absorption cross sections on arbitrarily shaped objects of sizes comparable to the lateral focus-extent (*e.g.*, single-walled carbon-nanotubes[10,27]) will fail as the general contribution of scattering and interference will change. The measured signal will strongly depend on the shape of the refractive index

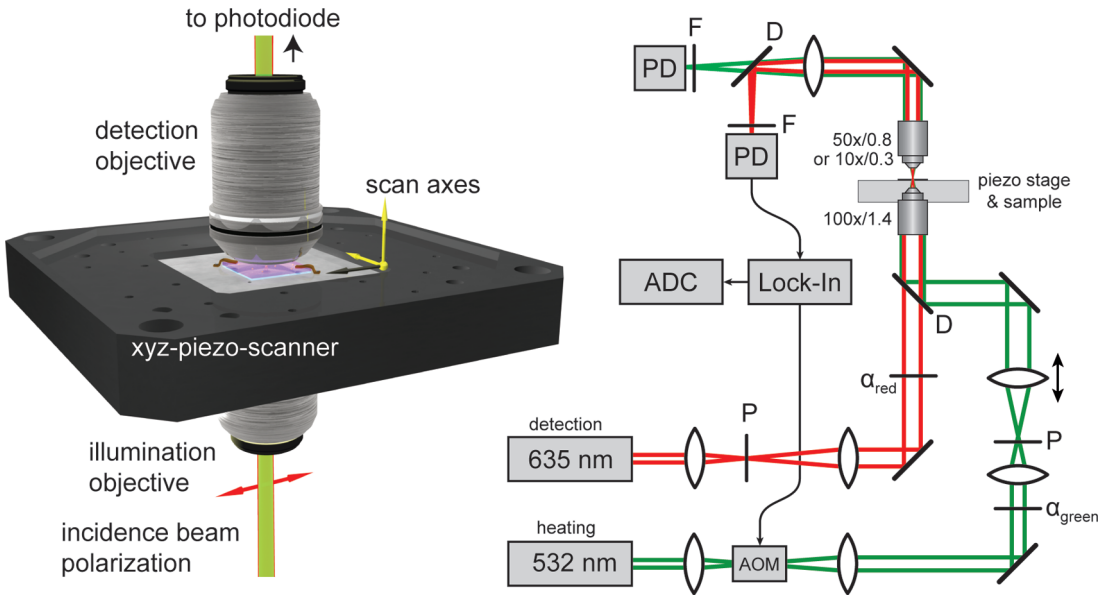

Figure 5. Principle scheme of the experimental setup: PD, photodiode detecting P_d; P, pinhole; D, dichroic mirror; F, filter; AOM, accusto-optic modulator; α, variable ND filter; ADC, Adwin analog digital converter.

profile even if the absorption cross section of the object is the same. A calibration will hence only give reasonable results when a comparing signal comes from the same type of spatial refractive index shapes (*i.e.*, inverse distance dependencies). However, this profile dependence may also be turned into an advantage as different transient and time-averaged refractive index profiles might be explored by anharmonic time dependencies of the heating laser modulation.[29]

The overall quality of our theoretical and experimental results is best displayed in Figure 3c,d, plotting the maximum and minimum photothermal signal values as well as their positions as a function of the axial focus displacement Δz_f. They show a perfect agreement of experiment (markers) and theory (lines) without the inclusion of fitting parameters. Moreover, they deliver a guideline, in which way the defocusing has to be adjusted to obtain a well-defined photothermal detection volume for an intended application of the technique. It also provides information on the location of the particle relative to the detection focus. This difference of the peak photothermal signal and probe or heating laser focus position has been observed before by comparing photothermal and fluorescence signals.[28] Following our theoretical treatment, it turns out that this difference in position is affected by the nanoparticle size and by aberrations. For particle radii smaller than 10 nm, the photothermal signal generated by a nonaberrated probe beam is vanishing if the particle is in the focus of the probe laser. The aberrated probe beam, however, leads to a finite signal at the particle position. This behavior is well understood in terms of the lensing action as well. While a nonaberrated beam is symmetric to the lens if directly focused to the center of the lens, the aberrated beam is not (Figure 4, left). The additional interference maxima of the incident field-intensity act like additional foci displaced with respect to the photothermal lens position and thus cause a photothermal signal. As a consequence, the displacement of particle fluorescence, which follows the heating beam intensity, and photothermal signal will depend on the aberration of the probe beam and not simply on the Gouy phase.[23] We have calculated three limiting cases with variable axial defocusing Δz_f, where either the positive lobe is maximal, both lobes show the same photothermal signal magnitude or the negative lobe is maximal (Figure 4, right). In the first case, photothermal and fluorescence signal maximum would be displaced by about 100 nm (top). In the second case, the zero-crossing of the photothermal signal coincides with the fluorescence maximum (center), while in the last case the fluorescence signal is almost exactly at the position of the photothermal signal minimum (bottom). Therefore, the commonly found displacements of fluorescence and photothermal signal[27,28] in the axial direction can be well explained by the presented theoretical approach and are plausible in the picture of a lensing action of the refractive index gradient.

CONCLUSION

We have presented experimental and theoretical results to demonstrate that the long-range refractive index change generated by a single heated nano-object in photothermal microscopy acts as a nanolens. The nanolens generates a dispersive signal along the optical axis separating a positive and negative photothermal focal volume. The ratio of positive and negative focal volume can be adjusted by displacing both heating and detection laser focus. A steady-state

generalized MIE description has been used to quantitatively understand the signal generation mechanism, which establishes photothermal microscopy as a quantitative technique to determine absolute absorption cross sections of single quantum objects and delivers a framework for new applications of this technique. As a direct consequence, new experimental techniques such as twin-focus photothermal correlation spectroscopy similar to the well-established dual focus fluorescence correlation techniques[30] or super-resolution absorption microscopy methods can be developed. We expect that the understanding of the photothermal signal generation will pave the way for further improvements of this technique beyond the current level of sensitivity.

METHODS

Sample Preparation. Our experimental studies have been carried out on gold nanoparticles (AuNP) embedded in a homogeneous polymer layer between two glass slides. Samples were prepared by spin-coating a polymer layer (Sylgard 184, about 15 μm thickness) on a glass-cover slide. AuNPs (BBI International) with a diameter of 60 nm were deposited on top of the polymer film. The particle size has been chosen to allow for a well detectable single-particle scattering signal. The particles were covered with a second Sylgard layer (also about 15 μm thick) to ensure the absence of a close-by interface and thus a radially symmetric temperature field around the particle.

Photothermal Microscopy Measurements. The experimental setup for single-particle light scattering and photothermal measurements is based on a home-built confocal sample-scanning microscopy setup using two laser sources. A DPSS laser (Coherent, Verdi) with λ_h = 532 nm is used to heat the gold particles and a second laser source at λ_d = 635 nm (Coherent ULN laser diode) probes the local refractive index changes. Both beams are focused into the sample by the same objective lens (Olympus 100×/1.4NA) and are collected above the sample by a second objective (Zeiss 10×/0.3NA or Olympus 50×/0.8NA), which is adjusted to image the probe focus to infinity (see Figure 5). The sample is moved by a piezo-scanner (PI, Physikalische Instrumente). The resulting parallel beam is focused onto two photodiodes (Thorlabs, PDA36A-EC) after passing appropriate filters (no pinhole). To allow for a low noise detection of the photothermal signal, the heating beam is modulated by an AOM (Isomet) with a frequency Ω = 300 kHz, and the probe signal modulation amplitude ΔV is detected at this reference frequency with a lock-in amplifier (Signal Recovery 7280 DSP) with a time constant of τ_{li} = 1 ms. The resulting lock-in signal is recorded by an A/D converter (Adwin-Gold, Jäger Messtechnik) 300 times within 1 ms for each recorded pixel (1 ms/pixel). The analyzed relative photothermal signal Φ corresponds to the modulation amplitude of the photovoltage ΔV at the photodiode

$$\Phi = \frac{\Delta V}{V} \tag{4}$$

relative to the background voltage V.

Single-Particle Light Scattering Measurements. Single-particle light scattering has been carried out in the same setup as the photothermal measurements. To do so, the intensity of heating and probe laser have been diminished such that no notable effects of varying incident laser power can be found in the experiments. The laser intensities of both wavelengths were recorded independently with two photodiodes (Thorlabs, PDA36A-EC) without intensity modulation and lock-in detection. All scattering signals have been normalized to the background intensity.

MIE Scattering Images. MIE scattering calculations were carried out with a modified version of the code from Peña et al.[24] The code implements the calculation of the far-field scattering coefficients for a multilayered scatterer, that is, the discretized refractive index profile. It has been modified to use new expressions (see Supporting Information) incorporating the incident field expansion coefficients for a given particle coordinate, the so-called beam shape coefficients of the GLMT. Further, the detection aperture NA_d has been introduced into the GLMT formalism calculating the integrated time-averaged Poynting vector $\langle \mathbf{S} \rangle_t$ (eq 3). This constitutes the energy-flux which is recorded by the photodiode in the forward scattering experiments in this study. The relative photothermal signal Φ is then calculated by taking the difference of single-particle scattering images in the presence and absence of the refractive index profile at the probe beam wavelength and subsequent normalization to the scattering background in the images without the refractive index profile. In all calculated images and signal profiles including the refractive index profile, the strength of the local refractive index change has been adjusted according to the thermorefractive coefficient $dn/dT = -3.6 \times 10^{-4}$ K^{-1} and particle temperature rise $\Delta T(r)$. The local temperature rise is evaluated from the absorbed heating laser power P_{abs}, which is obtained from the MIE calculations involving the focused heating laser and the nanoparticle at a well-defined position in the laser focus.

Conflict of Interest: The authors declare no competing financial interest.

Acknowledgment. Discussion with K. Kroy and D. Rings and financial support by the DFG research unit 877 and the graduate school BuildMoNa is acknowledged.

Supporting Information Available: A detailed description of the experimental setup, the material parameters, and the mathematical methods used. This material is available free of charge *via* the Internet at http://pubs.acs.org.

REFERENCES AND NOTES

1. Kulzer, F.; Orrit, M. Single-Molecule Optics. *Annu. Rev. Phys. Chem.* **2004**, *55*, 585–611.
2. Moerner, W. E.; Fromm, D. P. Methods of Single-Molecule Fluorescence Spectroscopy and Microscopy. *Rev. Sci. Instrum.* **2003**, *74*, 3597–3619.
3. Berciaud, S.; Cognet, L.; Blab, G.; Lounis, B. Photothermal Heterodyne Imaging of Individual Nonfluorescent Nanoclusters and Nanocrystals. *Phys. Rev. Lett.* **2004**, *93*, 257402.
4. Berciaud, S.; Cognet, L.; Lounis, B. Photothermal Absorption Spectroscopy of Individual Semiconductor Nanocrystals. *Nano Lett.* **2005**, *5*, 2160–3.
5. Harada, M.; Iwamotok, K.; Kitamori, T.; Sawada, T. Photothermal Microscopy with Excitation and Probe Beams Coaxial under the Microscope and Its Application to Microparticle Ananlysis. *Anal. Chem.* **1993**, *65*, 2938–2940.
6. Bialcowski, S. *Photothermal Spectroscopy Methods for Chemical Analysis*; John Wiley and Sons, Inc.: New York, 1996.
7. Boyer, D.; Tamarat, P.; Maali, A.; Lounis, B.; Orrit, M. Photothermal Imaging of Nanometer-Sized Metal Particles among Scatterers. *Science* **2002**, *297*, 1160–3.
8. Berciaud, S.; Lasne, D.; Blab, G.; Cognet, L.; Lounis, B. Photothermal Heterodyne Imaging of Individual Metallic Nanoparticles: Theory *versus* Experiment. *Phys. Rev. B* **2006**, *73*, 045424.
9. van Dijk, A. A.; Tchebotaareva, A. L.; Orrit, M.; Lippitz, M.; Berciaud, S.; Lasne, D.; Cognet, L.; Lounis, B. Absorption and Scattering Microscopy of Single Metal Nanoparticles. *Phys. Chem. Chem. Phys.* **2006**, *8*, 3486–3495.
10. Berciaud, S.; Cognet, L.; Lounis, B. Luminescence Decay and the Absorption Cross Section of Individual Single-Walled Carbon Nanotubes. *Phys. Rev. Lett.* **2008**, *101*, 077402.

11. Gaiduk, A.; Yorulmaz, M.; Ruijgrok, P. V.; Orrit, M. Room-Temperature Detection of a Single Molecule's Absorption by Photothermal Contrast. *Science* **2010**, *330*, 353–356.
12. Radünz, R.; Rings, D.; Kroy, K.; Cichos, F. Hot Brownian Particles and Photothermal Correlation Spectroscopy. *J. Phys. Chem. A* **2009**, *113*, 1674–1677.
13. Paulo, P. M. R.; Gaiduk, A.; Kulzer, F.; Krens, S. F. G.; Spaink, H. P.; Schmidt, T.; Orrit, M. Photothermal Correlation Spectroscopy of Gold Nanoparticles in Solution. *J. Phys. Chem. C* **2009**, *113*, 11451–11457.
14. Octeau, V.; Cognet, L.; Duchesne, L.; Lasne, D.; Schaeffer, N.; Fernig, D. G.; Lounis, B. Photothermal Absorption Correlation Spectroscopy. *ACS Nano* **2009**, *3*, 345–350.
15. Wähnert, M.; Radünz, R.; Cichos, F. Nanoscale Distance Fluctuations Probed by Photothermal Correlation Spectroscopy. *Proc. SPIE* **2009**, *7185*, 71850V.
16. Rings, D.; Schachoff, R.; Selmke, M.; Cichos, F.; Kroy, K. Hot Brownian Motion. *Phys. Rev. Lett.* **2010**, *105*, 090604.
17. Jurgensen, F.; Schroer, W. Studies on the Diffraction Image of a Thermal Lens. *Appl. Opt.* **1995**, *34*, 41–50.
18. Carslaw, H. S.; Jaeger, J. C. *Conduction of Heat in Solids*, 2nd ed.; Oxford University Press, USA, 1986.
19. Plech, A.; Kotaidis, V. Laser-Induced Heating and Melting of Gold Nanoparticles Studied by Time-Resolved X-ray Scattering. *Phys. Rev. B* **2004**, *70*, 195423.
20. Gouesbet, G.; Grehan, G.; Maheu, B. Scattering of a Gaussian-Beam by a MIE Scatter Center Using a Bromwich Formalism. *J. Opt.-Nouvelle Rev., D* **1985**, *16*, 83–93.
21. Neves, A. A. R.; Fontes, A.; Cesar, C. L.; Camposeo, A.; Cingolani, R.; Pisignano, D. Axial Optical Trapping Efficiency through a Dielectric Interface. *Phys. Rev. E* **2007**, *76*, 061917.
22. Nasse, M. J.; Woehl, J. C. Realistic Modeling of the Illumination Point Spread Function in Confocal Scanning Optical Microscopy. *J. Opt. Soc. Am. A* **2010**, *27*, 295–302.
23. Hwang, J.; Moerner, W. E. Interferometry of a Single Nanoparticle Using the Gouy Phase of a Focused Laser Beam. *Opt. Commun.* **2007**, *280*, 487–491.
24. Pena, O.; Pal, U. Scattering of Electromagnetic Radiation by a Multilayered Sphere. *Comput. Phys. Commun.* **2009**, *180*, 2348–2354.
25. Gouesbet, G.; Letellier, C.; Grehan, G.; Hodges, J. T. Generalized Optical Theorem for On-Axis Gaussian Beams. *Opt. Commun.* **1996**, *125*, 137–157.
26. Berg, M. J.; Sorensen, C. M.; Chakrabarti, A. Extinction and the Optical Theorem. Part I. Single Particles. *J. Opt. Soc. Am. A* **2008**, *25*, 1504–1513.
27. Giblin, J.; Syed, M.; Banning, M. T.; Kuno, M.; Hartland, G. Experimental Determination of Single CdSe Nanowire Absorption Cross Sections through Photothermal Imaging. *ACS Nano* **2010**, *4*, 358–364.
28. Gaiduk, A.; Ruijgrok, P. V.; Yorulmaz, M.; Orrit, M. Making Gold Nanoparticles Fluorescent for Simultaneous Absorption and Fluorescence Detection on the Single Particle Level. *Phys. Chem. Chem. Phys.* **2010**, *13*, 149–153.
29. Baffou, G.; Rigneault, H. Femtosecond-Pulsed Optical Heating of Gold Nanoparticles. *Phys. Rev. B* **2011**, *84*, 035415.
30. Dertinger, T.; Pacheco, V.; von der Hocht, I.; Hartmann, R.; Gregor, I.; Enderlein, J. Two-Focus Fluorescence Correlation Spectroscopy: A New Tool for Accurate and Absolute Diffusion Measurements. *Chem. Phys. Chem.* **2007**, *8*, 433–443.